MJFAS
Malaysian Journal of Fundamental and Applied Sciences

Fong *et al.* | Malaysian Journal of Fundamental and Applied Sciences, Vol. 22 (2026) 538-551

RESEARCH ARTICLE

Synthesis and Characterization of Polyaniline for the Removal of 4-Vinylcyclohexene in the Nitrile Glove Manufacturing Industry

Kar-Yan Fong[a], Rusli Daik[b], Sook-Wai Phang[a*]

[a]Department of Physical Science, Faculty of Applied Sciences, Tunku Abdul Rahman University of Management and Technology (TARUMT), 53300, Setapak, Kuala Lumpur, Malaysia; [b]Department of Chemistry Sciences, Faculty of Science and Technology, University Kebangsaan Malaysia (UKM), 43600, Bangi, Selangor, Malaysia

Abstract Volatile organic compounds (VOCs) are common by-products released during nitrile glove manufacturing, which can cause unpleasant odours and pose risks to human health and the environment. Among these VOCs, 4-vinylcyclohexene (4-VCH) is found to be emitted during production through cyclization of 1,3-butadiene. Polyaniline (PANI), which has been widely studied for the removal of pollutants, such as heavy metals and organic dyes, shows potential as an adsorbent for 4-VCH due to its tunable oxidation states. In this study, emeraldine salt (PANI-ES) was synthesized via chemical oxidation, while emeraldine base (PANI-EB) and pernigraniline base (PANI-PB) were obtained through deprotonation and further chemical oxidation. All synthesized PANI samples were examined using FTIR, UV-Vis, TGA and electrical conductivity measurements to confirm their chemical structures, oxidation states, thermal stability, and electrical properties. The adsorption performance of the different PANI oxidation states toward 4-VCH was determined using gas chromatography- flame ionization detector (GC-FID). Among the PANI samples, PANI-EB exhibited the highest 4-VCH removal efficiency of 19.21% at 60 mins in 100ppm 4-VCH solution, followed by PANI-PB with the removal efficiency of 17.75% at 90 mins, whereas PANI-ES showed the lowest removal efficiency of 13.53% at 60 mins. Post-adsorption UV-Vis and FTIR analyses revealed no significant changes in spectral features of PANI-EB, indicating that the adsorption mechanism is mainly by physical interactions. This study shows the potential of PANI, particularly in its emeraldine base form, as a potential adsorbent for the removal of non-polar VOCs, such as 4-VCH, from industrial emissions.

Keywords: Polyaniline, Volatile organic compounds, 4-vinylcyclohexene.

***For correspondence:**
phangsw@tarc.edu.my.

Received: 27 January 2026
Accepted: 25 May 2026

Introduction

The global glove market offers a range of different types of gloves, including latex, nitrile, and vinyl, each with distinct properties and applications. As a global leader in glove manufacturing, Malaysia has been recognised as the world's largest producer of latex and nitrile gloves. According to the report of Disposable Glove Global Market Insights 2024, during the COVID-19 pandemic, global glove production surged, with Malaysia manufacturing 85 billion and 67 billion pairs of rubber gloves in 2022 and 2023, respectively. In the 1990s, latex gloves dominated the market, but growing concerns over latex allergies eventually led to a gradual shift toward nitrile gloves [1]. This shift was driven by nitrile gloves, offering lower allergy risks, greater tear resistance, and more affordable compared to latex gloves [2]. Despite

these advantages, the manufacturing of nitrile gloves relies on synthetic rubber, specifically nitrile butadiene rubber derived from 1,3-butadiene and acrylonitrile, which has been associated with the formation of volatile organic compound (VOC) by-products. The presence of 1,3-butadiene allows side reactions such as cyclization, resulting in the formation of cyclohexene derivatives, including 4-vinylcyclohexene [3-4]. Although studies on VOC emissions from glove manufacturing remain limited, evidence from related rubber industries, such as tyre production, has proven that cyclohexene derivatives can be produced in butadiene-based processes, showing a potential environmental concern associated with large-scale nitrile glove production.

Volatile organic compounds (VOCs) are carbon-based pollutants with low boiling points, high vapour pressures and volatilities. VOCs can be classified into anthropogenic and naturally occurring VOCs, where anthropogenic VOCs are mainly emitted from human activities, such as vehicle exhaust, fuel combustion and various industrial activities, while naturally occurring VOCs are produced and emitted from biogenic compounds like plants and microorganisms [5]. Common VOCs include aromatic hydrocarbons, such as benzene and toluene, as well as aliphatic hydrocarbons like ethane and hexene, along with alcohols, aldehydes, ketones, esters and ethers [6]. These VOCs are readily emitted into the atmosphere, causing significant air pollution, and several of these compounds have been suspected or proven to be carcinogenic, thereby posing serious risks to human health. Hence, the development of effective strategies for VOCs removal is crucial. Existing VOC mitigation approaches are generally classified into destructive and recovery methods. Destruction methods, including catalytic oxidation, thermal incineration, biofiltration and photocatalytic oxidation, aim to break down VOCs into less or non-harmful by-products such as carbon dioxide and water. However, these approaches usually require high temperatures and optimum conditions to achieve maximum removal efficiency. In contrast, recovery techniques, such as adsorption, condensation, membrane separation and absorption, focus on separating and capturing VOCs by changing the process conditions like temperature and pressure [7]. Among these techniques, adsorption is preferable in this study due to its operational simplicity, energy efficiency, high removal efficiency even at low concentrations, and its ability to prevent the generation of secondary pollutants as compared to other destructive methods.

Industrial activities are one of the principal sources of emitting VOCs, particularly from petrochemical industries, polymer manufacturing, as well as paint and coating industries [8-10]. Among these, the rubber glove manufacturing industry is of particular interest in this research study, as Malaysia is one of the largest global producers and exporters of rubber gloves. If unreacted or excess chemicals are present during the production of nitrile gloves, by-products may be generated and released into the atmosphere, resulting in environmental pollution. Of particular concern is 4-vinylcyclohexene (4-VCH), a volatile alicyclic hydrocarbon that can be generated as a by-product during the dimerization of 1,3-butadiene [3]. 4-VCH has been identified as potentially carcinogenic and toxic to reproductive health and is classified as a hazardous air pollutant by the U.S. Environmental Protection Agency (EPA). Moreover, the presence of 4-VCH releases an unpleasant odour, which is undesirable in the glove manufacturing process [11]. Despite these concerns, studies focusing on its removal remain limited compared to other common VOCs, such as benzene and toluene. Therefore, in this research study, the removal of 4-VCH using PANI as an adsorbent will be investigated.

Polyaniline (PANI) is one of the most widely studied conducting polymers due to its reversible redox properties, various oxidation states, unique functional groups, tunable conductivity and ease of synthesis. PANI can exist in three main oxidation states of leucoemeraldine, emeraldine, and pernigraniline, each associated with different colours. In its fully reduced state, leucomeraldine appears colourless or white and consisting only benzenoid units in its molecular structure. The partially oxidized form, emeraldine, shows blue colour and consists of both benzenoid and quinonoid units, while the fully oxidized form, perniganiline, is violet and consists solely of quinonoid units [12]. Of these, the emeraldine form is considered the most valuable due to its high environmental stability at room temperature and reversible transition between conducting and insulating states. Furthermore, PANI has been extensively applied as an adsorbent in removing various pollutants, including heavy metals and organic dyes, with emeraldine salt being the most commonly applied form owing to the presence of protonated amine sites (–NH+) along the polymer backbone. The presence of protonated quinoid groups and benzenoid structures in the emeraldine salt allows effective pollutant adsorption through electrostatic interactions between -NH+ in PANI and negatively charged pollutants, hydrogen bonding between nitrogen (N) in PANI and electronegative atoms (oxygen, nitrogen, fluorine), as well as π-π interaction between conjugated benzene in PANI and aromatic compounds [13]. In comparison to conventional adsorbents such as activated carbon and zeolite, PANI was selected due to its relatively simple synthesis through chemical oxidation polymerization, lower synthesis cost, and its potential regeneration ability through simple chemical treatments using acid/base eluents [14]. To date, although no studies have focused on the removal of cyclohexene-based compounds using PANI as an adsorbent, the tunable oxidation states

and diverse interaction mechanisms of PANI show potential for the adsorption of 4-VCH, where different oxidation states of PANI may exhibit distinct removal efficiencies.

In this research, PANI powder adsorbents with different oxidation states, specifically emeraldine salt, emeraldine base and perniganiline base, are synthesized and evaluated for the effective removal of 4-VCH under varying contact times, as illustrated in Figure 1. To date, no studies have reported the adsorption of cyclohexene-related compounds, potential by-products generated during glove manufacturing, using PANI powder adsorbents. By investigating the adsorption performance of different PANI oxidation states, this study aims to provide new findings into the feasibility of PANI as a sustainable adsorbent for VOC mitigation in industrial applications.

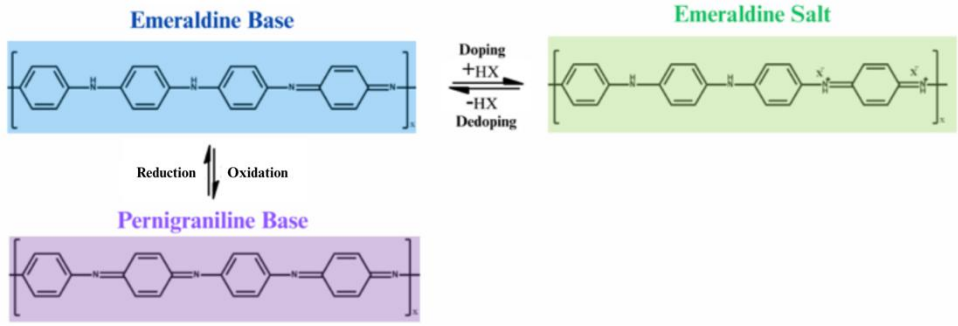

Figure 1. Chemical structures of different oxidation states of PANI

Materials and Methods

For the synthesis of emeraldine salt of PANI (PANI-ES), aniline (ANI, 99.5% purity) was used as the monomer and hydrochloric acid (HCl, 37.0% purity) was used as the acidic dopant, both purchased from R & M Chemicals. Ammonium persulfate (APS, 98.0% purity) served as the oxidant and methanol (99.8% purity) for washing was purchased from Sigma Aldrich, while acetone was from Bendosen Laboratory Chemicals. Ammonium hydroxide solution (purity = 30.0%) from R & M Chemicals was used to deprotonate PANI-ES to emeraldine base of PANI (PANI-EB). For the removal experiments, 4-vinylcyclohexene (4-VCH, 97.0% purity) and *n*-hexane (≥98.0% purity) were used for the preparation of standard solutions, both purchased from Sigma Aldrich. During the characterization of PANI using UV-Visible (UV-Vis) spectroscopy, dimethyl sulfoxide (DMSO, 99.9% purity) from Fisher Scientific was used as the solvent. All chemicals were of analytical reagent (AR) grade, while n-hexane was gas chromatography (GC) grade. Distilled water from a simple distillation setup was used throughout the project.

PANI synthesis

PANI was synthesized using HCl as an acidic dopant and APS as an oxidant. Initially, 0.2 M ANI/HCl solution was prepared and cooled to 0 °C. Polymerization of PANI was initiated by the dropwise addition of APS solution into the ANI/HCl solution under constant stirring at 0 °C. The reaction mixture was stirred for 2 hours at 0 °C, followed by continuous stirring for an additional 24 hours at the same temperature. After polymerization, the resulting green PANI powder in emeraldine salt (PANI-ES) form was washed thrice using 1.0 M HCl, followed by acetone to remove any unreacted monomers and impurities. The sample was then collected via vacuum filtration and oven dried at 60 °C for a day. After drying, PANI-ES was ground into fine powder and placed in a desiccator for moisture control. PANI in emeraldine base (PANI-EB) form was prepared from PANI-ES via deprotonation using 1.0 M ammonium hydroxide solution. The deprotonation process was terminated once the green PANI-ES turned blue PANI-EB. The resulting PANI-EB was washed thoroughly with distilled water and methanol, followed by vacuum filtration and oven drying at 60 °C for 24 h. PANI in pernigraniline base form (PANI-PB) was synthesized via further chemical oxidation of PANI-EB using 0.1 M APS solution. The oxidation process was stopped upon the formation of the violet colour of PANI-PB. The obtained PANI-PB was then washed with distilled water and methanol, collected by vacuum filtration, and vacuum dried at 40 °C for 24 h.

Characterization of PANI

Attenuated Total Reflectance Fourier Transform Infrared (ATR-FTIR) spectroscopy (Perkin Elmer Spectrum 100) was used to study the chemical structures and functional groups of each synthesized PANI-ES, PANI-EB and PANI-PB over a wavenumber range of 4000 - 650 cm^{-1}, with 16 scans recorded for each spectrum at room temperature. Ultraviolet-Visible (UV-Vis) spectroscopy (Hitachi UH5300 Double Beam Spectrophotometer) was used to determine the oxidation states of the PANI samples within a wavelength range of 300 - 1000 nm, using dimethyl sulfoxide (DMSO) as the solvent. Thermogravimetric analysis (TGA) was performed using a TGA Q50 Instrument to evaluate the thermal stability of each PANI sample. The analysis was performed from room temperature to 900°C at a heating rate of 20°C/min under nitrogen atmosphere with a flow rate of 50 mL/min. Electrical conductivity of each PANI sample was measured using a low resistivity meter (Mitsubishi Loresta GX MCP-T700). Each sample was compressed into a 13 mm diameter pellet using a digital hydraulic press (PIKE Technologies) under a force of 10 tons at room temperature, with a thickness ranging from 0.4761 mm to 0.6361 mm, measured using a digital micrometer (Mitutoyo) prior to conductivity measurements using a four-point PSP probe.

Volatile organic compound (VOC) removal

1000 ppm stock solution of 4-VCH was prepared by dissolving the compound in *n*-hexane, followed by serial dilution to obtain standard 4-VCH solutions of desired concentrations. The concentrations of the 4-VCH solutions were analysed using gas chromatography equipped with a flame ionization detector (GC-FID) (Shimadzu GC-2010 Plus). A calibration curve was plotted using the prepared standard solutions. For adsorption studies, 100 mg of different PANI samples (PANI-ES, PANI-EB, and PANI-PB) was added to a 100 ppm 4-VCH solution. The adsorption process was performed under continuous shaking at 200 rpm at room temperature for contact times ranging from 15 to 120 min to evaluate the adsorption behaviour of PANI towards 4-VCH [15]. A blank control experiment without PANI was carried out under identical experimental conditions to account for possible 4-VCH loss due to evaporation. After adsorption, the mixtures were centrifuged and filtered, and the filtrates were analysed using GC-FID to determine the remaining 4-VCH concentration. The VOC removal efficiency (%) of the PANI samples at different contact times was calculated using Equation (1):

$$\text{VOC Removal efficiency (\%)} = \frac{C_I - C_F}{C_I} \times 100\% \quad (1)$$

where C_I is the initial concentration of 4-VCH before adsorption (ppm), and C_F is the final concentration of 4-VCH after adsorption (ppm).

Proposed adsorption mechanism between PANI-EB and 4-VCH

Post-adsorption characterization was carried out only on PANI-EB, as it exhibited the highest 4-VCH removal efficiency among the different oxidation states. After adsorption for 60 min, PANI-EB was filtered and oven-dried overnight at 60 °C. The dried PANI-EB sample was subsequently characterized using UV-Vis and FTIR spectroscopy to investigate any changes in oxidation state and chemical structure after the adsorption of 4-VCH, as well as to evaluate the interactions involved between PANI-EB and 4-VCH during adsorption.

Results and Discussion

FTIR analysis

FTIR analysis was conducted to confirm the functional groups and chemical structure of each synthesized PANI sample in the wavenumber range of 4000 cm^{-1} to 600 cm^{-1}. Figure 2 shows the FTIR spectra of (a) PANI-ES, (b) PANI-EB and (c) PANI-PB. As shown in Figure 2, the absorption bands observed at 3207 cm^{-1}, 3253 cm^{-1} and 3243 cm^{-1} represent the N-H stretching vibration, while the peaks at 2905 cm^{-1}, 2922 cm^{-1} and 2918 cm^{-1} are attributed to aromatic C-H stretching in PANI-ES, PANI-EB and PANI-PB, respectively [16-17]. Next, in the FTIR spectrum of PANI-ES, the prominent absorption bands at 1554 cm^{-1} and 1435 cm^{-1} are attributed to the C=C stretching vibrations of the quinoid and benzenoid units, respectively. In comparison, the corresponding peaks for PANI-EB are observed at 1582 cm^{-1} and 1495 cm^{-1}, while PANI-PB exhibits corresponding peaks at 1574 cm^{-1} and 1485 cm^{-1} [18]. The presence of conjugated quinoid and benzenoid structures in PANI may facilitate interactions with unsaturated 4-VCH molecules through Van der Waals forces and π-interactions during the adsorption. Furthermore, absorption bands due to the C-N stretching of the secondary aromatic amine were observed at 1283 cm^{-1}, 1307 cm^{-1} and 1316 cm^{-1} for PANI-ES, PANI-EB and PANI-PB, respectively. Lastly, characteristic absorption bands corresponding to aromatic C-H in-plane bending vibrations are observed at 1033 cm^{-1}, 1160 cm^{-1}, and 1145 cm^{-1}, while the aromatic C–H out-of-plane bending

vibrations are present at 782 cm^{-1}, 744 cm^{-1}, and 798 cm^{-1} for PANI-ES, PANI-EB, and PANI-PB, respectively [18].

The differences in the positions and intensities of the quinoid and benzenoid absorption bands among PANI-ES, PANI-EB, and PANI-PB show variations in the oxidation state of PANI. In particular, the relative intensities of the quinoid and benzenoid stretching vibration bands can be used as an indicator of the oxidation level of the polymer [19]. As shown in Figure 2, the intensity ratio of the quinoid to benzenoid bands in PANI-PB is higher than both PANI-ES and PANI-EB, owing to the higher intensity of the quinoid stretching vibration observed for PANI-PB. This can be attributed to the increased presence of quinoid units resulting from further oxidation of PANI-EB to PANI-PB, thereby resulting in a higher oxidation level of the PANI backbone [19].

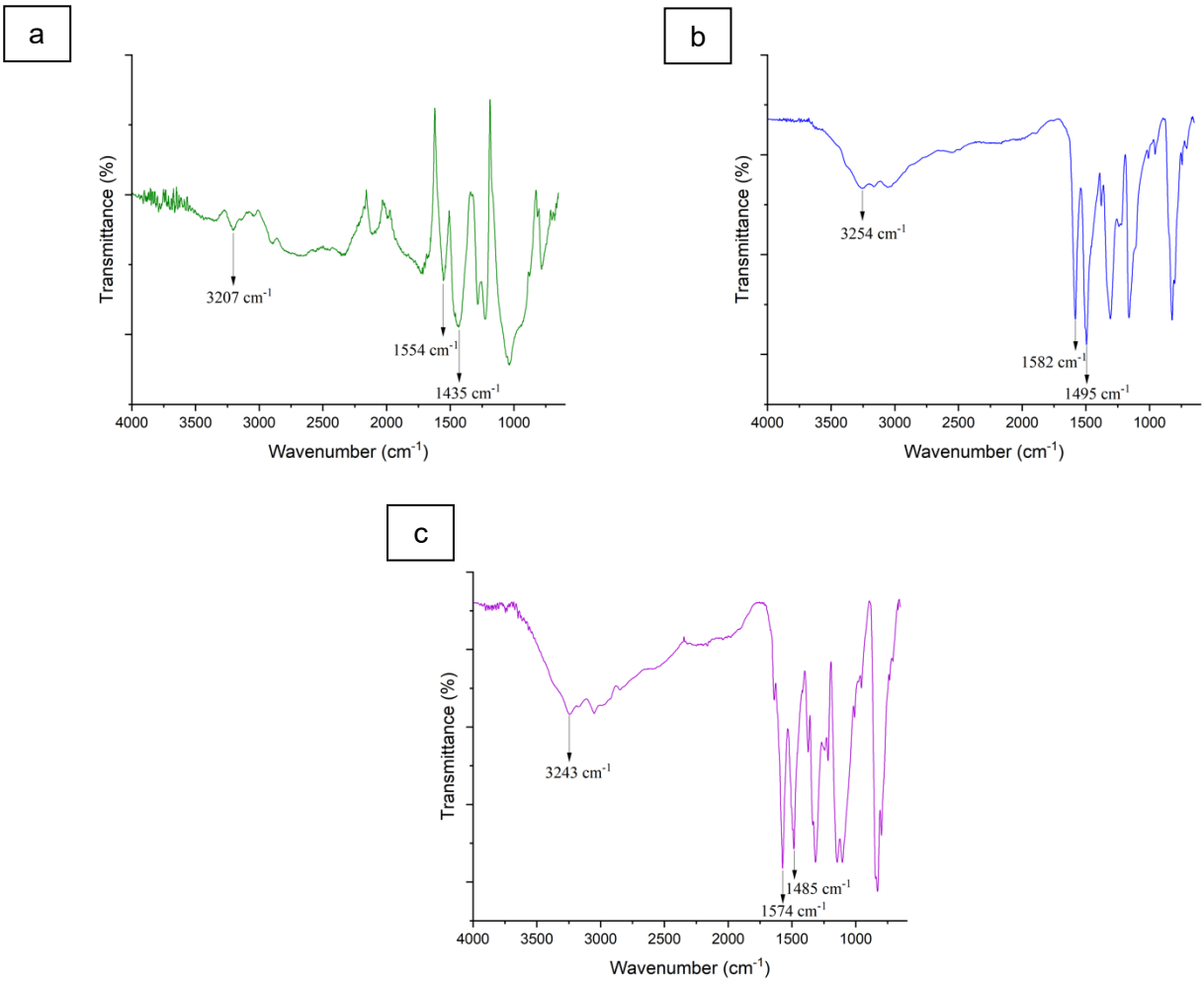

Figure 2. FTIR spectra of (a) PANI-ES, (b) PANI-EB, and (c) PANI-PB.

UV-Vis analysis

UV-Vis spectroscopy is used to determine the oxidation states of each synthesized PANI sample. Figure 3 shows the UV-Vis absorption spectra of (a) PANI-ES, (b) PANI-EB and (c) PANI-PB from 300 nm to 1000 nm. Distinct absorption peaks corresponding to different electronic transitions were observed for each oxidation state of PANI. PANI-ES exhibited three characteristic absorption bands, whereas PANI-EB and PANI-PB showed two significant absorption peaks, indicating differences in the electronic structures associated with protonation and oxidation levels. For PANI-ES, the absorption peak at 330 nm is attributed to the $\pi \rightarrow \pi^*$ transition in the benzenoid ring, while the absorption band at 444 nm corresponds to the polaron $\rightarrow \pi^*$ transition in the protonated quinoid segments of PANI-ES [19-20]. In addition, a broad free carrier tail from around 742 nm is observed, indicating the $\pi \rightarrow$ polaron transition in the synthesized PANI-ES. The presence of polaron transitions in PANI-ES indicates enhanced electronic delocalization along the conjugated polymer backbone, confirming that PANI has been

successfully synthesized in its protonated, electrically conducting ES state [21].

On the other hand, the UV-vis spectrum of PANI-EB exhibited an absorption band at 328 nm, indicating the π → π* transition of the benzenoid units. A second absorption band observed at 628 nm corresponds to the excitonic transition between the benzenoid and quinoid segments of PANI, which shows the characteristic of PANI-EB [22]. In comparison, the UV-Vis spectrum of PANI-PB showed a similar overall absorption pattern due to its non-protonated nature. An absorption peak at 316 nm is attributed to the π → π* transition of the conjugated PANI-PB backbone, and the broad absorption band at around 600 to 620 nm corresponds to π → π* transition in quinoid units, showing the higher oxidation state of pernigraniline [17]. The differences in the electronic transitions observed among each synthesized PANI show variations in the degree of electron delocalization within the polymer backbone, which may influence the interaction between PANI and 4-VCH molecules during adsorption.

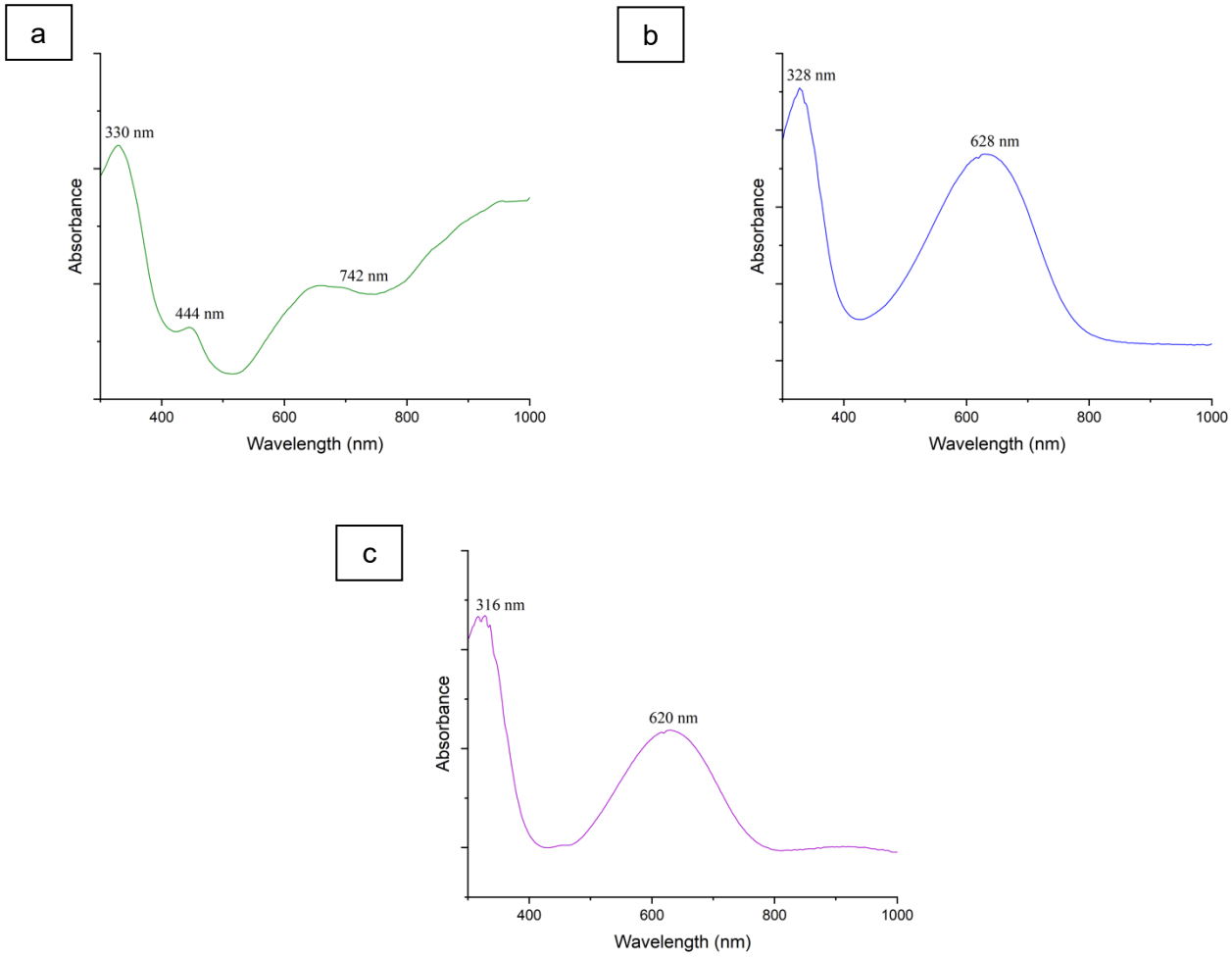

Figure 3. UV-Vis spectra of (a) PANI-ES, (b) PANI-EB, and (c) PANI-PB.

TGA analysis

TGA was carried out to determine the thermal stability of each synthesized PANI when subjected to elevated temperature in a controlled environment. Figure 4 compares the thermal stability of PANI-ES, PANI-EB, and PANI-PB through TGA thermograms. As shown in the thermogram, PANI-ES exhibits three main decomposition stages, with the first stage occurring below 130 °C, exhibiting a weight loss of 14.17%. This is attributed to the loss of the adsorbed moisture within the polymer matrix as well as residual unreacted monomer. The second decomposition stage is observed between 150 °C and 300 °C, with a weight loss of 11.11%, corresponding to the loss of HCl acidic dopant and the degradation of low molecular weight oligomers present in the polymer matrix [23]. The third decomposition stage, occurring between 430 °C and 620 °C, is mainly associated with the decomposition of the PANI-ES

polymer backbone [24]. During this stage, a weight loss of 28.94% was observed.

In contrast, both PANI-EB and PANI-PB exhibit only two main decomposition stages, which can be attributed to the absence of HCl acidic dopants in the polymer backbones, thereby eliminating the decomposition stage of acidic dopants observed in PANI-ES. The first decomposition stage in both PANI-EB and PANI-PB was observed below 100 °C, with weight losses of 8.79% and 8.41%, respectively. This indicates the evaporation of adsorbed moisture and residual solvents within the polymer matrix of both PANI-EB and PANI-PB. The second decomposition stage, associated with the degradation of the polymer backbone, occurs at approximately 450 °C, with weight losses of 36.10% for PANI-EB and 26.42% for PANI-PB.

Based on Figure 4, PANI-PB exhibits higher apparent thermal stability compared to PANI-EB and PANI-ES. Although both PANI-EB and PANI-PB decompose at a higher temperature than PANI-ES, PANI-PB shows the highest residual weight of 48.79%, followed by PANI-EB (42.51%) and PANI-ES (32.62%). The higher char residue of PANI-PB indicates an enhanced thermal stability under high temperature conditions. The observed differences in thermal stability can be attributed to the different oxidation states of PANI. The lower thermal stability of PANI-ES than PANI-EB is mainly attributed to the presence of acidic dopants, which disrupt thermal transitions within the polymer backbone due to chain decomposition, as reported by Yalcin and co-researchers [25]. In addition, although PANI-PB has been reported to exhibit lower intrinsic stability due to its fully oxidized quinoid structure, the present results show that PANI-PB exhibits the highest residual weight [12]. This may be attributed to thermal reduction of PANI-PB toward the more thermodynamically stable PANI-EB form at elevated temperatures.

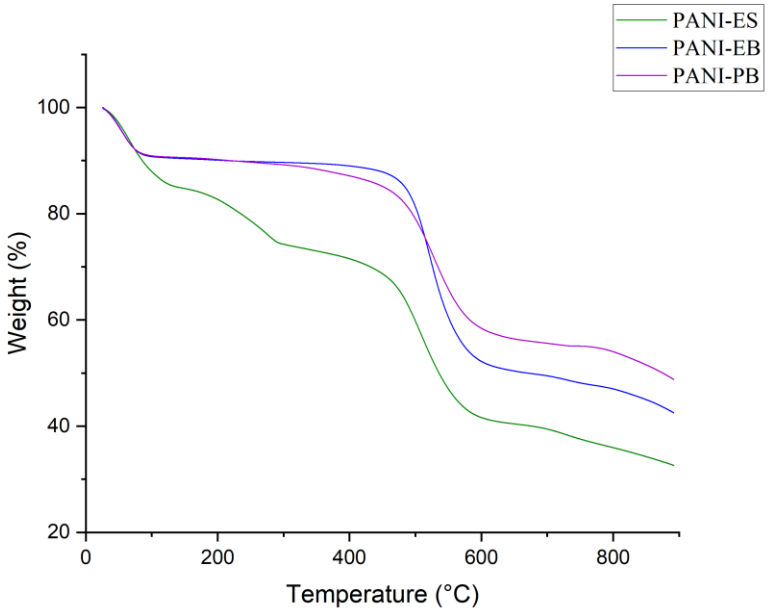

Figure 4. Thermogram of PANI-ES, PANI-EB, and PANI-PB.

Electrical conductivity measurement

Table 1 shows the electrical conductivity of the synthesized PANI-ES, PANI-EB, and PANI-PB measured using a four-point PSP probe. Among the three samples, only PANI-ES exhibited measurable electrical conductivity, with a value of 8.50 ± 1.42 S/cm. The relatively high conductivity of PANI-ES is mainly attributed to the protonic doping effect of HCl and the low-temperature polymerization process carried out at 0 °C [26]. Polymerization at low temperature promotes more ordered chain growth slowly and steadily, which facilitates charge transport along the conjugated polymer backbone and improves electrical conductivity [27].

In contrast, PANI-EB and PANI-PB showed an “Over Load” response during measurement, indicating that the resistivity exceeded the maximum measurable limit of the instrument of 10^7 Ω. This suggests that both PANI-EB and PANI-PB possess very low electrical conductivity compared to PANI-ES. The low conductivity of PANI-EB and PANI-PB is due to the absence of HCl acidic dopants, which are needed for protonation of the imine nitrogen atoms to generate charge carriers of polarons and bipolarons along the PANI backbone, thereby allowing effective charge transport [26].

Table 1. The electrical conductivity of PANI-ES, PANI-EB and PANI-PB.

Sample	Electrical Conductivity (S/cm)
PANI-ES	8.50 ± 1.42
PANI-EB	< Detection Limit
PANI-PB	< Detection Limit

**Detection limit corresponds to a resistivity exceeding 10^7 Ω.*

4-VCH Removal Efficiency

Figure 5 shows the removal efficiency of 4-VCH using different oxidation states of PANI (PANI-ES, PANI-EB, and PANI-PB) at contact times ranging from 15 to 120 min. As shown in Figure 5, the removal efficiency of 4-VCH increases gradually with increasing contact time from 15 to 60 min for all PANI samples. For PANI-ES, the removal efficiency increases from 3.76% to 13.53%. Similarly, the removal efficiency for PANI-EB increases from 9.66% to 19.21%, while that of PANI-PB increases from 3.57% to 11.27% over the same contact time interval. After 60 min, the removal efficiency of 4-VCH for PANI-EB decreased from 19.21% to 12.47% at 90 min and further dropped to 8.42% at 120 min, while PANI-ES exhibited removal efficiencies of 11.39% and 13.10% at contact times of 90 min and 120 min, respectively. On the other hand, for PANI-PB, the removal efficiency continued to increase to 17.75% at 90 min, followed by a decrease to 9.20% at 120 min.

Initially, the increase in removal efficiency with contact time could be attributed to the availability of abundant active adsorption sites on each PANI surface [28]. This allows effective interaction between 4-VCH molecules and PANI. As the contact time increases, the active sites on PANI gradually become saturated, causing the adsorption process to approach equilibrium. As a result, weakly adsorbed 4-VCH molecules may gradually desorb back into the solution, resulting in a decrease in removal efficiency after 60 min [29-30]. Since the adsorption of 4-VCH onto PANI is mainly governed by weak physical interactions, the adsorption is likely reversible at prolonged contact times.

Among the different oxidation states, PANI-EB exhibited the highest removal efficiency of 19.21% at 60 min. This can be attributed to the stable oxidation state as well as the neutral backbone structure of PANI-EB. In PANI-EB, the deprotonated amine and imine groups provide a relatively non-polar surface that facilitates favourable interaction with non-polar 4-VCH molecules, leading to more effective adsorption compared to PANI-ES and PANI-PB [31]. In contrast, the presence of HCl acidic dopants in PANI-ES may hinder interactions with non-polar 4-VCH, as the presence of the positively charged -NH+- sites is unfavourable for the adsorption of non-polar molecules. Moreover, the availability of adsorption sites in PANI-ES may be reduced due to the protonation of imine groups, thereby resulting in a lower removal efficiency. For the highly oxidized and quinoid-rich PANI-PB, the removal efficiency was found to be higher than that of PANI-ES but lower than that of PANI-EB. This can be due to the more rigid polymer backbone and the increased of quinoid unit in PANI-PB, which may limit the chain flexibility and reduce the accessibility of active sites for non-polar 4-VCH molecules [32].

GC-FID was used to evaluate the concentration of 4-VCH before and after adsorption by comparing the peak areas of 4-VCH before and after adsorption with different PANI samples. During the adsorption process, n-hexane was used as the solvent. The preferential adsorption of 4-VCH over n-hexane onto the active sites of PANI during the adsorption stage may be attributed to the stronger interactions between 4-VCH and each PANI sample. Based on the GC chromatograms shown in Figure 6 and the peak area data in Table 2, the peak area of n-hexane at a retention time of around 6.3 min showed minimal reduction throughout the adsorption process for 60 min, whereas a more significant decrease was observed for 4-VCH at a retention time of approximately 7.9 min, indicating that 4-VCH was preferentially adsorbed by PANI-EB. This behaviour may be associated with the molecular structure of 4-VCH, which contains unsaturated C=C bonds that may interact with the conjugated benzenoid and quinoid structures of PANI-EB through π-interactions in addition to Van der Waals forces [30, 33]. In contrast, n-hexane mainly interacts with PANI through relatively weak Van der Waals forces due to its saturated aliphatic structure [34-35]. Hence, 4-VCH shows a higher affinity toward PANI-EB during the adsorption.

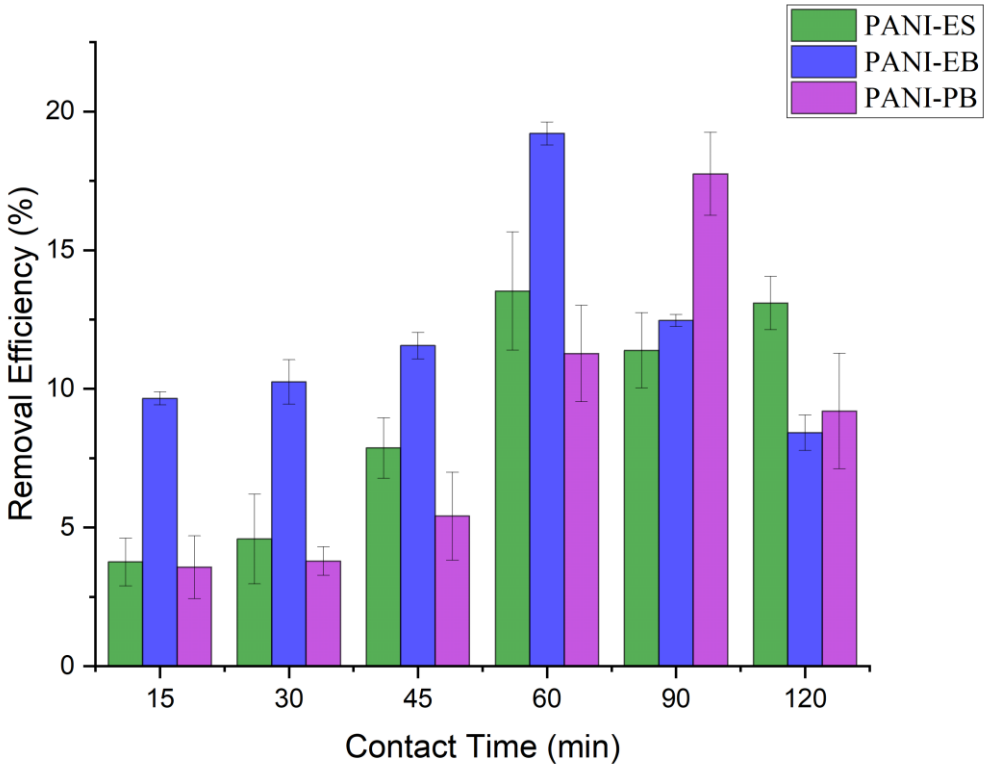

Figure 5. Comparison of 4-VCH removal efficiency with PANI-ES, PANI-EB, and PANI-PB at varying contact times.

a

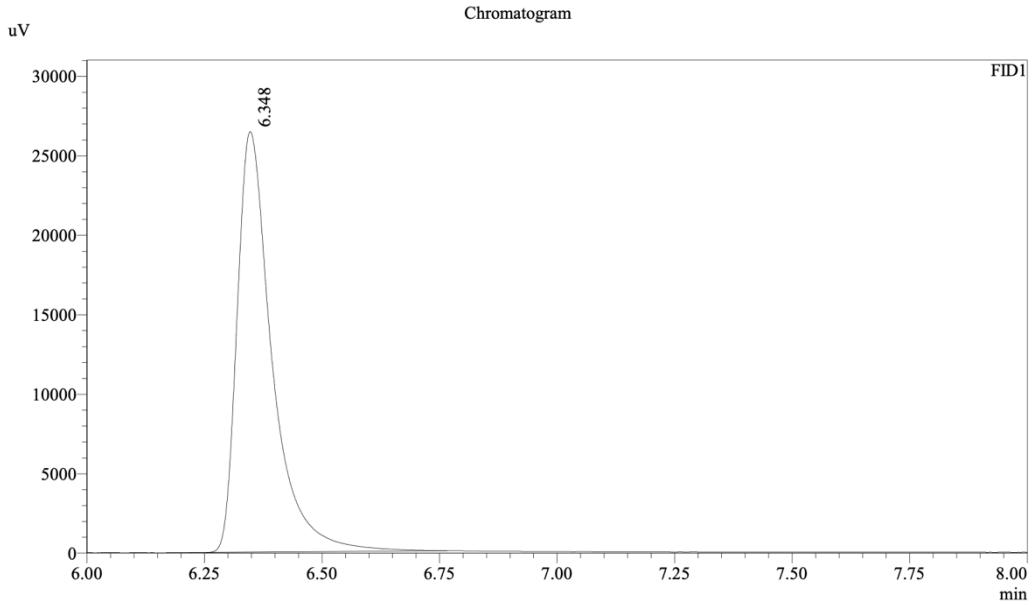

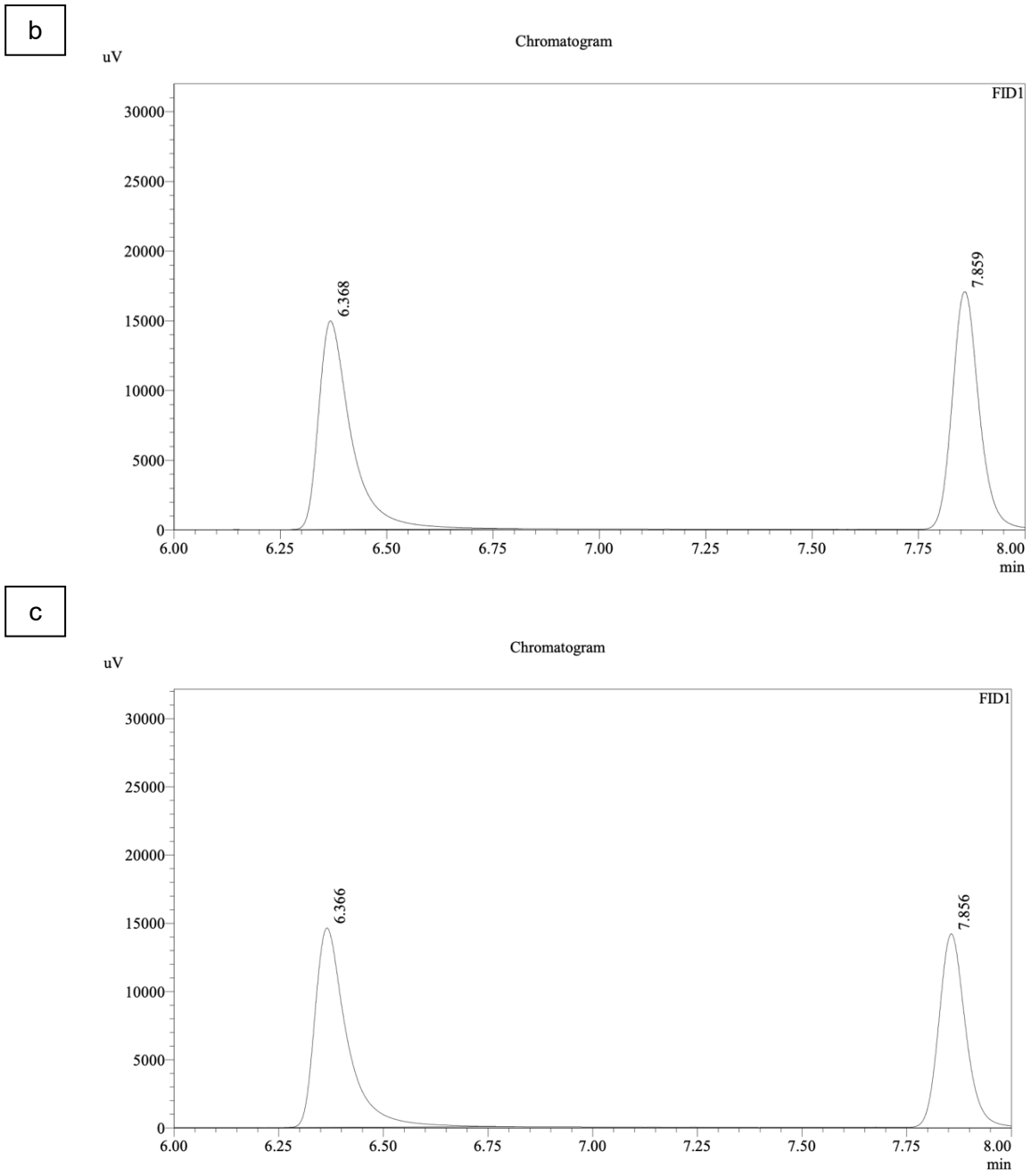

Figure 6. GC chromatograms in the retention time region of 6 - 8 min for (a) pure n-hexane, (b) 4-VCH solution without PANI-EB after 60 min shaking, and (c) 4-VCH solution with PANI-EB after 60 min shaking.

Table 2. Comparison of GC peak areas for n-hexane and 4-VCH before and after adsorption using PANI-EB for 60 min.

Compound	Retention Time (min)	Peak Area Without PANI-EB	Peak Area With PANI-EB	Reduction (%)
n-hexane	~ 6.3	79603	77885	2.16
4-VCH	~ 7.9	74769	62491	16.42

Proposed adsorption mechanism between PANI-EB and 4-VCH

Post-adsorption analyses of PANI-EB via FTIR and UV-Vis were conducted to evaluate the interactions involved between PANI-EB and 4-VCH during adsorption. As shown in Figures 7 and 8, no significant changes in characteristic absorption bands and peak positions were observed after 4-VCH adsorption. From Figure 7, the UV-Vis spectrum of PANI-EB after 4-VCH adsorption shows a slight decrease in absorbance intensity, suggesting that the interaction between PANI-EB and 4-VCH occurred during the adsorption [36]. This reduction in absorbance intensity may be attributed to minor perturbations in electron distribution along the conjugated PANI-EB backbone upon the interaction between PANI-EB and 4-VCH molecules, thereby resulting in a decrease in electron delocalization [21, 37]. However, no new absorption bands or peak shifts were observed after the adsorption of 4-VCH, indicating that the electronic structure and oxidation state of PANI-EB remained unchanged.

Similarly, the FTIR spectra before and after adsorption show similar characteristic peaks, indicating that the chemical structure of PANI-EB remains intact after adsorption. The absence of new functional group vibrations further confirms that no new chemical bonds were formed between PANI-EB and 4-VCH [36, 38-39]. In addition, the volatile 4-VCH may have partially desorbed during the post-adsorption drying process, thereby resulting in minimal spectral changes. Based on these results, the interaction between PANI-EB and 4-VCH is mainly by physical adsorption mechanisms, including Van der Waals forces and π-interactions, rather than chemisorption [36,40].

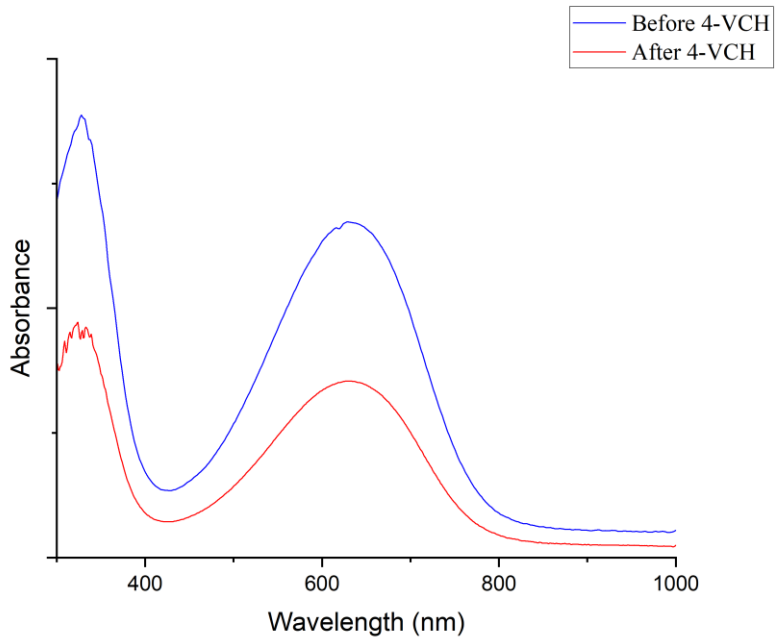

Figure 7. Comparison of UV-Vis spectra of PANI-EB before and after 4-VCH adsorption.

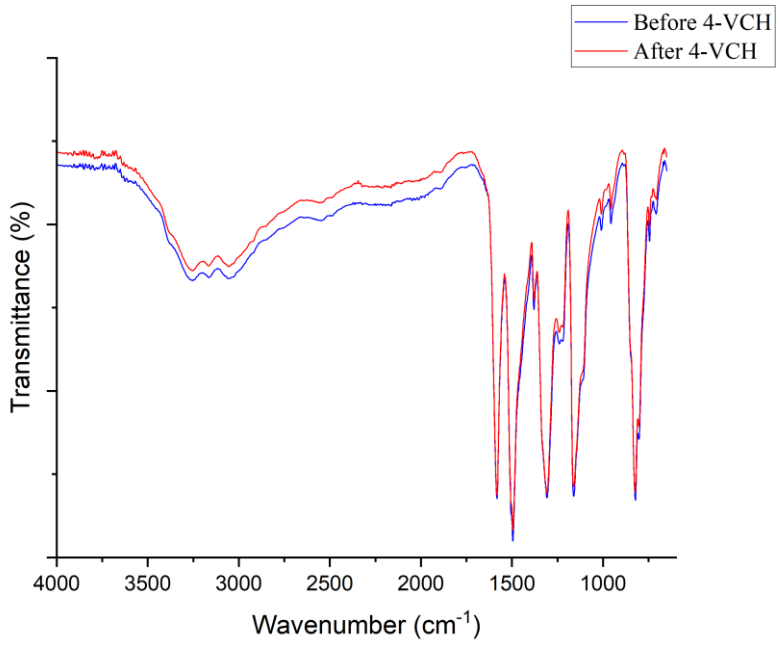

Figure 8. Comparison of FTIR spectra of PANI-EB before and after 4-VCH adsorption.

With this, a plausible adsorption mechanism between PANI-EB and 4-VCH was proposed in Figure 9 to study the interaction behaviour. Owing to the neutral polymer backbone and absence of charged functional groups in PANI-EB, it provides favourable interaction sites for non-polar 4-VCH molecules through Van der Waals forces [31]. In addition, 4-VCH can be adsorbed onto the active sites of PANI-EB via weak π-interactions through the interaction between the C=C double bonds in 4-VCH and the aromatic rings of PANI-EB [39].

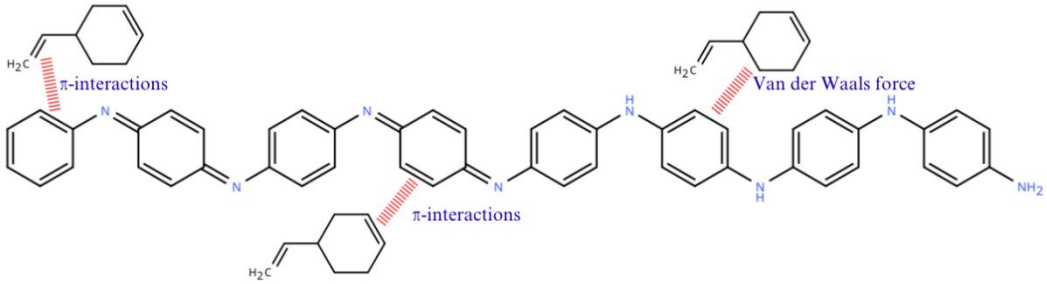

Figure 9. Proposed adsorption mechanism between PANI-EB and 4-VCH.

Conclusions

In conclusion, this research study shows the potential of PANI with different oxidation states, synthesized via chemical oxidation and deprotonation, for the removal of non-polar 4-VCH through adsorption. All synthesized PANI samples were successfully characterized using FTIR, UV-Vis, TGA, and electrical conductivity measurements to investigate their chemical structures, oxidation states, thermal stability, and electrical properties. Subsequently, the removal efficiency of 4-VCH by PANI-ES, PANI-EB and PANI-PB was examined using GC-FID. Among the different oxidation states, PANI-EB exhibited the highest removal efficiency of 19.21% at a contact time of 60 min in 100 ppm 4-VCH solution. This enhanced performance is due to its neutral polymer backbone, which facilitates favourable interactions with non-polar 4-VCH molecules through Van der Waals forces and weak π-interactions. Furthermore, post-adsorption FTIR and UV-Vis analyses of PANI-EB revealed no significant changes in spectral features, indicating that the adsorption of 4-VCH is dominated by physical interactions rather than chemisorption.

Conflicts of Interest

The authors declare that there is no conflict of interest regarding the publication of this paper.

Acknowledgment

This work is part of a research project supported by Tunku Abdul Rahman University of Management and Technology (TAR UMT).

References

[1] Nucera, E., Aruanno, A., Rizzi, A., & Centrone, M. (2020). Latex Allergy: Current Status and Future Perspectives. Journal of Asthma and Allergy, Volume 13, 385–398.
[2] Gunasegaran, J., Teh, Y.-Y., Lim, C.-K., & Ng, S.-F. (2024). Review on Prevalence, Risk Factors, and Research Advancements on the Use of Medical Gloves Concerning Hand Dermatitis Among Health Care Workers. Safety and Health at Work, 15(2), 129–138.
[3] Huang, Y., Shen, L., Ma, C., Jiang, Y., & Yu, B. (2024). Functionalization of 1,3-Butadiene Derivatives under Photo/Electrocatalysis. European Journal of Organic Chemistry, 27(28).
[4] Schulze, W. T., Schwalbe, S., Trepte, K., Croy, A., Kortus, J., & Gräfe, S. (2023). Bond formation insights into the Diels–Alder reaction: A bond perception and self-interaction perspective. The Journal of Chemical Physics, 158(16).
[5] Zhou, X., Zhou, X., Wang, C., & Zhou, H. (2023). Environmental and human health impacts of volatile organic compounds: A perspective review. Chemosphere, 313, 137489.
[6] David, E., & Niculescu, V.-C. (2021). Volatile Organic Compounds (VOCs) as Environmental Pollutants: Occurrence and Mitigation Using Nanomaterials. International Journal of Environmental Research and Public Health, 18(24), 13147.
[7] Zhu, L., Shen, D., & Luo, K. H. (2020). A critical review on VOCs adsorption by different porous materials: Species, mechanisms and modification methods. Journal of Hazardous Materials, 389, 122102.
[8] Ding, Z., Li, Y., Fu, Q., Tian, M., Wang, F., Wang, Y., & Huang, K. (2025). Volatile organic compounds in a typical petrochemical production area in Shanghai, China: Source profiles, human health and environmental impacts. Environmental Pollution, 372, 126074.
[9] Huang, H., Wang, Z., Dai, C., Guo, J., & Zhang, X. (2022). Volatile organic compounds emission in the rubber products manufacturing processes. Environmental Research, 212, 113485.
[10] Mo, Z., Lu, S., & Shao, M. (2021). Volatile organic compound (VOC) emissions and health risk assessment in paint and coatings industry in the Yangtze River Delta, China. Environmental Pollution, 269, 115740.
[11] Meng, J., Wang, J., Ning, X., Li, W., Wang, G., Li, W., Ma, B., Wang, J., Wang, H., Xiao, X., Cui, H., & Jing, B. (2024). Olfactory-chemical establishment using odour wheels and fingerprints to manage odor pollution for the petrochemical industry. Microchemical Journal, 205, 111253.
[12] Beygisangchin, M., Abdul Rashid, S., Shafie, S., Sadrolhosseini, A. R., & Lim, H. N. (2021). Preparations, Properties, and Applications of Polyaniline and Polyaniline Thin Films—A Review. Polymers, 13(12), 2003.
[13] Sowa, I., Wójciak, M., Tyszczuk-Rotko, K., Klepka, T., & Dresler, S. (2022). Polyaniline and Polyaniline-Based Materials as Sorbents in Solid-Phase Extraction Techniques. Materials, 15(24), 8881.
[14] Samadi, A., Xie, M., Li, J., Shon, H., Zheng, C., & Zhao, S. (2021). Polyaniline-based adsorbents for aqueous pollutants removal: A review. Chemical Engineering Journal, 418, 129425.
[15] Arsalan, M., Siddique, I., Awais, A., Baoji, M., Khan, I., Badran, M., & Mousa, A. A. A. (2022). Highly Efficient PANI-WH Novel Composite for Remediation of Ni(II), Pb(II), and Cu(II) From Wastewater. Frontiers in Environmental Science, 10.
[16] Jamadade, V. S., Dhawale, D. S., & Lokhande, C. D. (2010). Studies on electrosynthesized leucoemeraldine, emeraldine and pernigraniline forms of polyaniline films and their supercapacitive behavior. Synthetic Metals, 160(9–10), 955–960.
[17] Xie, M., Kim, J. W., Yang, Z., Uemura, S., Anderson, M., Katsuyama, Y., Kroes, B. C., Chang, X., Lin, C.-W., & Kaner, R. B. (2025). Heterophase Reduction of the Fully Oxidized Aniline Tetramer. ACS Materials Letters, 7(2), 675–681.
[18] Ajeel, K. I., & Kareem, Q. S. (2019). Synthesis and Characteristics of Polyaniline (PANI) Filled by Graphene (PANI/GR) nano-Films. Journal of Physics: Conference Series, 1234, 012020.
[19] Yoon, S.-B., Yoon, E.-H., & Kim, K.-B. (2011). Electrochemical properties of leucoemeraldine, emeraldine, and pernigraniline forms of polyaniline/multi-wall carbon nanotube nanocomposites for supercapacitor applications. Journal of Power Sources, 196(24), 10791–10797.
[20] Udum, Y. A., Killard, A. J., & Wagner, M. (2024). Determination of the relative sensitivity of polyaniline inks and films to deprotonation by ammonia using UV–Vis spectroscopy. European Polymer Journal, 205, 112709.
[21] Goswami, S., Nandy, S., Calmeiro, T. R., Igreja, R., Martins, R., & Fortunato, E. (2016). Stress Induced Mechano-electrical Writing-Reading of Polymer Film Powered by Contact Electrification Mechanism. Scientific Reports, 6(1), 19514.
[22] Passador, F. R., de Faria, P. v., Backes, E. H., Montanheiro, T. L. A., Montagna, L. S., de Souza Pinto, S., Pessan, L. A., & Rezende, M. C. (2017). Thermal, mechanical and electromagnetic properties of LLDPE/PANI composites. Polymer Bulletin, 74(7), 2701–2717.
[23] Lenin, R., Singh, A., & Bera, C. (2021). Effect of dopants and morphology on the electrical properties of

polyaniline for various applications. Journal of Materials Science: Materials in Electronics, 32(20), 24710–24725.
[24] Sayah, A., Boumaza, N., Habelhames, F., Bahloul, A., Tounsi, A., Lamiri, L., & Nessark, B. (2024). Effect of dopant on electrochemical performance of polyaniline on FTO substrate. Polymer Bulletin, 81(6), 5179–5192.
[25] Yalcin, D., Bamford, S., Espiritu, M., Rigopoulos, N., Martinez-Botella, I., Alexander, D., Gozukara, Y., Greaves, M., Bruton, E. A., Kinlen, P. J., Howard, S., Pigram, P. J., Muir, B. W., & Kohl, T. M. (2023). New insight into degradation mechanisms of conductive and thermally resistant polyaniline films. Polymer Degradation and Stability, 215, 110427.
[26] Toroń, B., Das, T. K., Kozioł, M., Szperlich, P., & Kępińska, M. (2025). Impact of hydrochloric acid doping on polyaniline conductivity and piezoelectric performance in polyaniline/bismuth oxyiodide nanocomposites. Composites Part B: Engineering, 289, 111960.
[27] Banjar, M. F., Joynal Abedin, F. N., Fizal, A. N. S., Muhamad Sarih, N., Hossain, Md. S., Osman, H., Khalil, N. A., Ahmad Yahaya, A. N., & Zulkifli, M. (2023). Synthesis and Characterization of a Novel Nanosized Polyaniline. Polymers, 15(23), 4565.
[28] Michelle, L.-Y. L., Ahmad, I., & Phang, S.-W. (2024). Preparation and Optimization of Polyaniline/ Titanium Dioxide/ Carboxymethyl Cellulose Powder for Effective Nickel Adsorption. Sains Malaysiana, 53(7), 1661–1676.
[29] Nath, B. K., Chaliha, C., Kalita, E., & Kalita, M. C. (2016). Synthesis and characterization of ZnO:CeO2:nanocellulose:PANI bionanocomposite. A bimodal agent for arsenic adsorption and antibacterial action. Carbohydrate Polymers, 148, 397–405.
[30] Li, X., Zhang, L., Yang, Z., Wang, P., Yan, Y., & Ran, J. (2020). Adsorption materials for volatile organic compounds (VOCs) and the key factors for VOCs adsorption process: A review. Separation and Purification Technology, 235, 116213.
[31] Khan, M. I., Almesfer, M. K., Elkhaleefa, A., Shigidi, I., Shamim, M. Z., Ali, I. H., & Rehan, M. (2021). Conductive Polymers and Their Nanocomposites as Adsorbents in Environmental Applications. Polymers, 13(21), 3810.
[32] Liao, G., Li, Q., & Xu, Z. (2019). The chemical modification of polyaniline with enhanced properties: A review. Progress in Organic Coatings, 126, 35–43.
[33] Benabdesselam, S., Sellami, M. H., Ghomri, R., Mezouar, M., & Amor, A. A. (2024). Removal of benzene and toluene from aqueous solutions using Phoenix dactylifera leaves treated with HNO3 as adsorbent: Kinetic, isotherm studies and modeling. Desalination and Water Treatment, 320, 100668.
[34] Wobowiec, M., Muir, B., Bajda, T., Zięba, K., Kijak, B., & Franus, W. (2017). Removal of BTEX and hexane by organo-zeolites: The influence of surfactant carbon chain length on the sorption process. Desalination and Water Treatment, 94, 120–128.
[35] Ojaghloo, L., Assadi, A., Mohammadian Fazli, M., & Peyda, M. (2025). Removal of n-hexane extractable material from synthetic oil produced water using Desmopan®5377A thermoplastic polyurethane packed bed reactor. Environmental Health Engineering and Management, 12, 1416.
[36] Mohamad Ahad, I. Z., Wadi Harun, S., Gan, S. N., & Phang, S. W. (2018). Polyaniline (PAni) optical sensor in chloroform detection. Sensors and Actuators B: Chemical, 261, 97–105.
[37] Albuquerque, J. E., Mattoso, L. H. C., Balogh, D. T., Faria, R. M., Masters, J. G., & MacDiarmid, A. G. (2000). A simple method to estimate the oxidation state of polyanilines. Synthetic Metals, 113(1–2), 19–22.
[38] Hussin, H., Gan, S.-N., & Phang, S.-W. (2021). Development of water-based polyaniline sensor for hydrazine detection. Sensors and Actuators A: Physical, 317, 112460.
[39] Abdelraheem, A., H. El-Shazly, A., & Elkady, M. (2019). Comparable investigation of polyaniline behavior towards gaseous ammonia and toluene adsorption. Environmental Science and Pollution Research, 26(4), 3991–3999.
[40] Choi, J.-S., Lim, S.-H., Lingamdinne, L. P., Park, S.-Y., Koduru, J. R., Yang, J.-K., & Chang, Y.-Y. (2023). Development of ultra-high surface area polyaniline-based activated carbon for the removal of volatile organic compounds from industrial effluents. Environmental Pollution, 337, 122594.